Target Diagnostics Package for the Light Ion Beam Fusion Target Development Facility

G.A. Moses, R.R. Peterson, M.E. Sawan and E.G. Lovell

September 1984

UWFDM-593

FUSION TECHNOLOGY INSTITUTE

UNIVERSITY OF WISCONSIN

MADISON WISCONSIN

Target Diagnostics Package for the Light Ion Beam Fusion Target Development Facility

G.A. Moses, R.R. Peterson, M.E. Sawan and E.G. Lovell

Fusion Technology Institute
University of Wisconsin
1500 Engineering Drive
Madison, WI 53706

http://fti.neep.wisc.edu

September 1984

UWFDM-593

TARGET DIAGNOSTICS PACKAGE FOR THE LIGHT ION BEAM FUSION TARGET DEVELOPMENT FACILITY

G.A. Moses

R.R. Peterson

M.E. Sawan

E.G. Lovell

Fusion Technology Institute
Nuclear Engineering Department
University of Wisconsin-Madison
Madison, Wisconsin 53706

September 1984

UWFDM-593

1. Introduction

The Light Ion Fusion Target Development Facility[1] must be equipped with target diagnostics that give the experimenter information regarding the details of the target implosion and burn. These diagnostic instruments will be different from those used today for low yield targets. In today's target experiments the energy yield is low enough that the target output can be used directly as the signal for the diagnostics without destroying the diagnostics on each shot. This is in contrast to underground weapons tests where the diagnostics are destroyed on a single shot. The TDF is likely to be in between these two extremes. The diagnostics instruments must be designed to survive from one to maybe fifty shots without refurbishment. The design of these diagnostics is of course difficult without detailed knowledge of the target designs. However, there is likely to be good reason to put a diagnostics "package" into the reaction vessel and place it near the target as shown in Fig. 1. The question then becomes, what environment does this package see and can it be designed to survive?

The TDF has been designed for the purpose of developing and testing high yield targets with nominal yields in the range of 50 to 200 MJ. The reaction chamber that contains these ~ 100 MJ explosions is 3 meters in radius and is filled with ~ 10 torr of gas such as argon or nitrogen. This gas is necessary to support the formation of z-pinch plasma channels to allow propagation of the ion beams from individual diodes behind the chamber first wall to the target.[2] The exploding target releases about 70% of its thermonuclear energy in the form of high energy neutrons and gamma rays. The remainder of the energy is in the form of x-rays and expanding ions. This energy is partially attenuated or stopped by the chamber gas, resulting in the formation of a

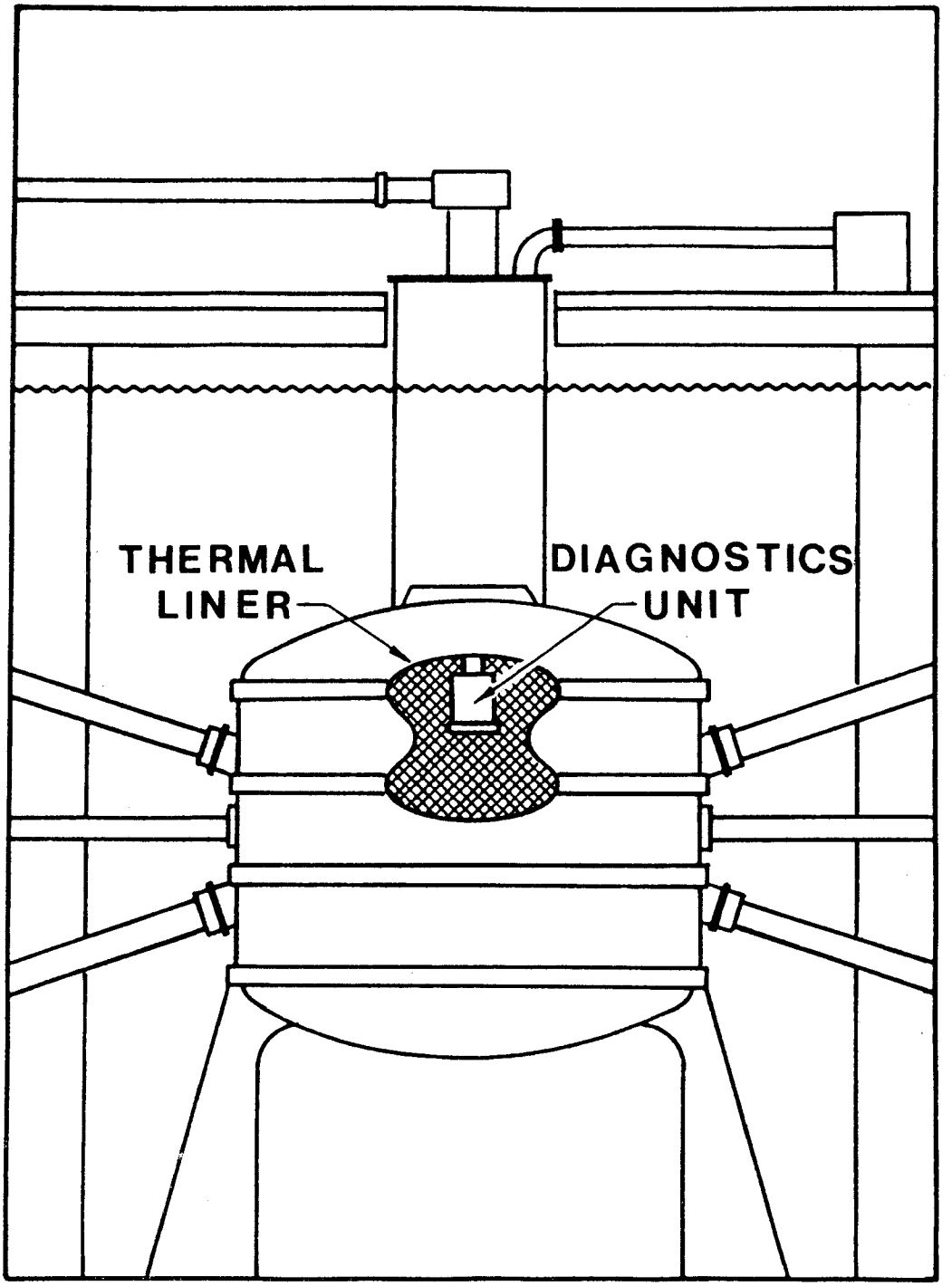

Fig. 1. Schematic of diagnostics package.

fireball. This fireball propagates to the first wall and subjects it to a surface heat flux and overpressure.[3-5]

A diagnostic package internal to the first wall will be exposed to at least 5 forms of radiation:

1. Neutrons,
2. Prompt target gamma rays,
3. Prompt target x-rays,
4. Fireball thermal x-rays, and
5. EMP.

We have investigated the first four of these forms for a particular light ion fusion target design.[6] We look at the problem for two types of chamber gas: (1) 10 torr of argon, and (2) 10 torr of nitrogen. The overpressure loading on the face of the diagnostics package is computed and representative faceplate designs are given. We compute the attenuation of radiation through the faceplate. In the last section of the report we present some ideas regarding possible target diagnostic methods applicable to the TDF.

2. Light Ion Fusion Target

The light ion fusion target used in this study was originally designed and reported by Bangerter.[6] It was slightly modified during the HIBALL study[7] and the modified target is shown in Fig. 2. In this diagram we show the target in its initial configuration and also in its configuration at the time of ignition. This ignition state was estimated from the reported yield of 113 MJ. Using this final configuration as our initial condition we simulated the thermonuclear burning of the fuel and the hydrodynamic disassembly of the target using the PHD-IV hydrodynamics-thermonuclear burn-radiative transfer computer code.[8] We also did an independent neutron transport

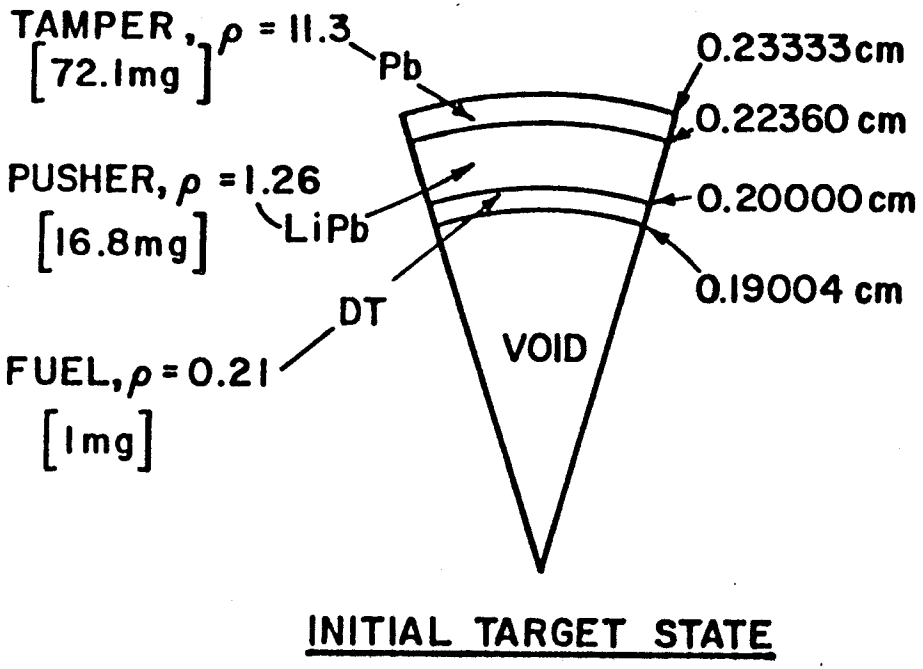

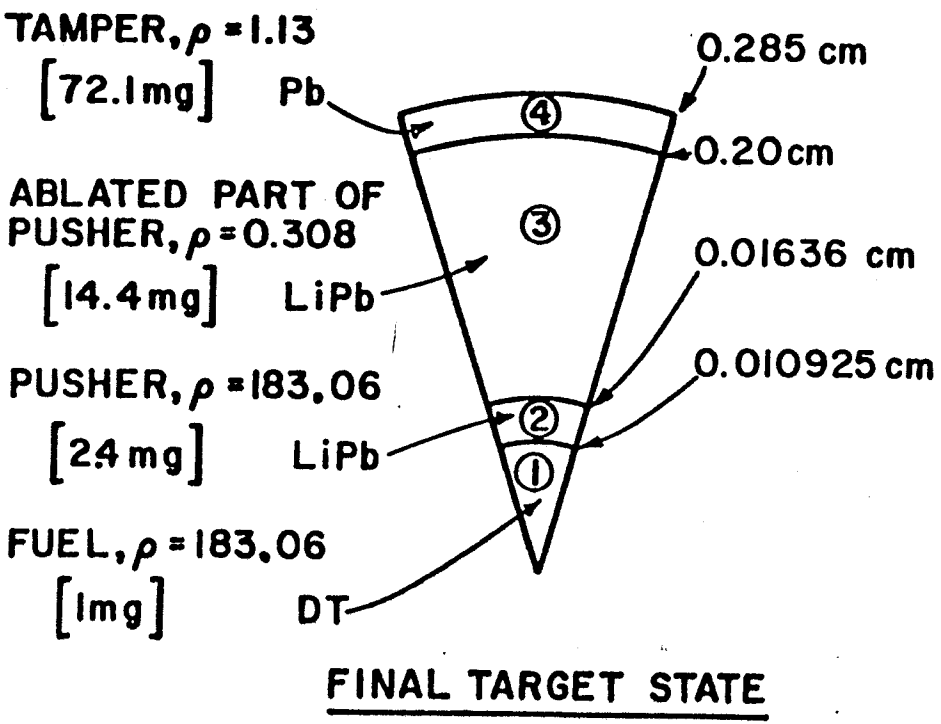

Fig. 2. LIB target configuration.

calculation for this compressed target using the ANISN code[9] to estimate the spectrum of neutrons and gamma rays escaping from the target. These hydrodynamic and transport calculations are reported elsewhere.[7,10] Using these two calculations we estimate the energy partitioning of the target to be that shown in Table 1. The results are normalized to a yield of exactly 200 MJ for convenience. This represents an extrapolation of the published results but is probably well within the accuracy of these calculations. The neutron spectrum from the target is shown in Fig. 3 and the gamma ray spectrum is shown in Fig. 4. The x-ray spectrum is shown in Fig. 5. The partitioning of the ion energy between the different species is given in Table 2. These results now serve as input to the fireball calculations discussed in the next section.

3. Fireball Calculations

When the light ion beam fusion target explodes in a gas-filled chamber the x-rays emitted by the target are attenuated by the gas. Likewise, the expanding ionic debris is stopped in the gas, creating a fireball. This fireball propagates to the first wall imparting an overpressure. The gas also reradiates a portion of the energy that it absorbs and this represents a thermal heat flux on the first wall. This thermal loading and overpressure will also affect any diagnostics that are located within the reaction chamber. In this section we present results of calculations that estimate these quantities.

The fireball calculations were done using the MF-FIRE multifrequency radiation-gas dynamics computer code.[11] The physical properties of the gas were computed using the MIXERG multifrequency opacity and equation of state computer code.[12] Using the MF-FIRE code we can calculate the prompt x-ray attenuation in the gas and the unattenuated x-rays reaching the first wall. The energy deposited by the attenuated x-rays gives an initial temperature

Table 1. Energy Partitioning of the Light Ion Fusion Target

Neutrons	141.5 MJ
γ-rays	0.30 MJ
x-rays	46 MJ
Ion Debris	10.2 MJ
Endothermic	2 MJ
	200 MJ

Table 2. Partitioning of Energy Between Ion Species

Species	Energy/Ion	Energy/Species
D	1.2 keV/ion	0.032 MJ
T	1.76 keV/ion	0.048 MJ
He^4	2.34 keV/ion	0.026 MJ
Li	4.1 keV/ion	0.76 MJ
Pb	121. keV/ion	9.33 MJ
		10.2 MJ

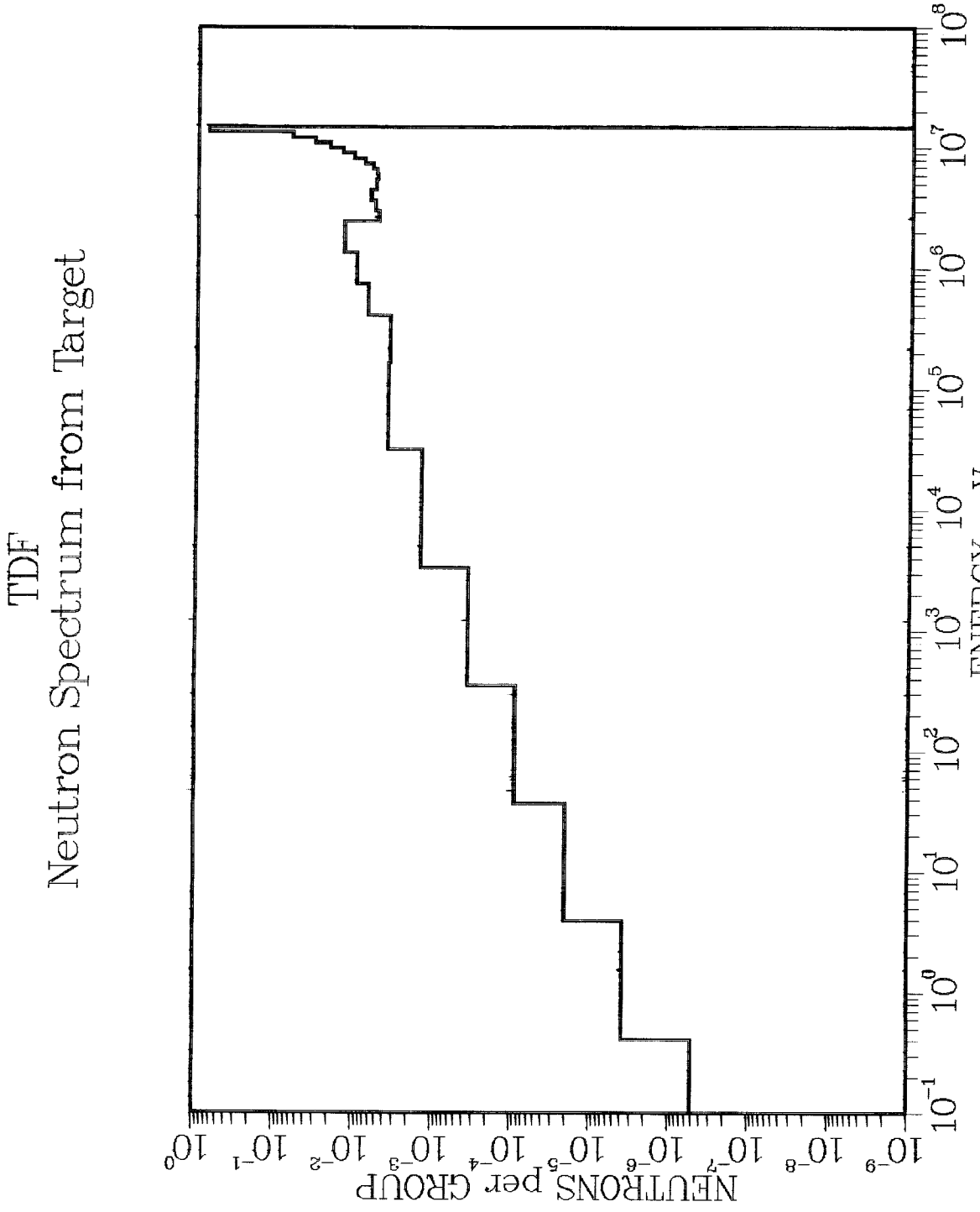

Fig. 3. LIB target neutron spectrum.

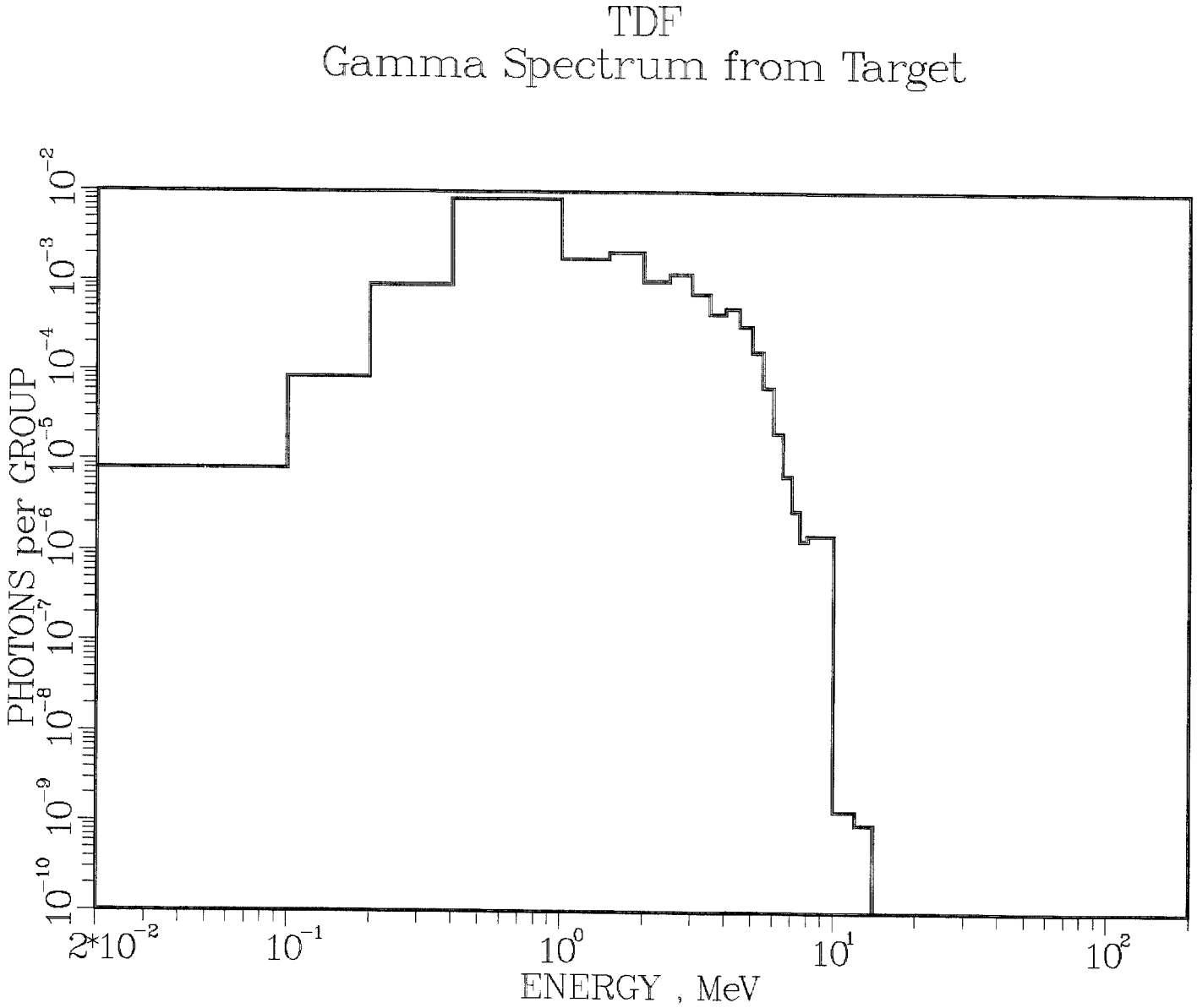

Fig. 4. LIB target gamma ray spectrum.

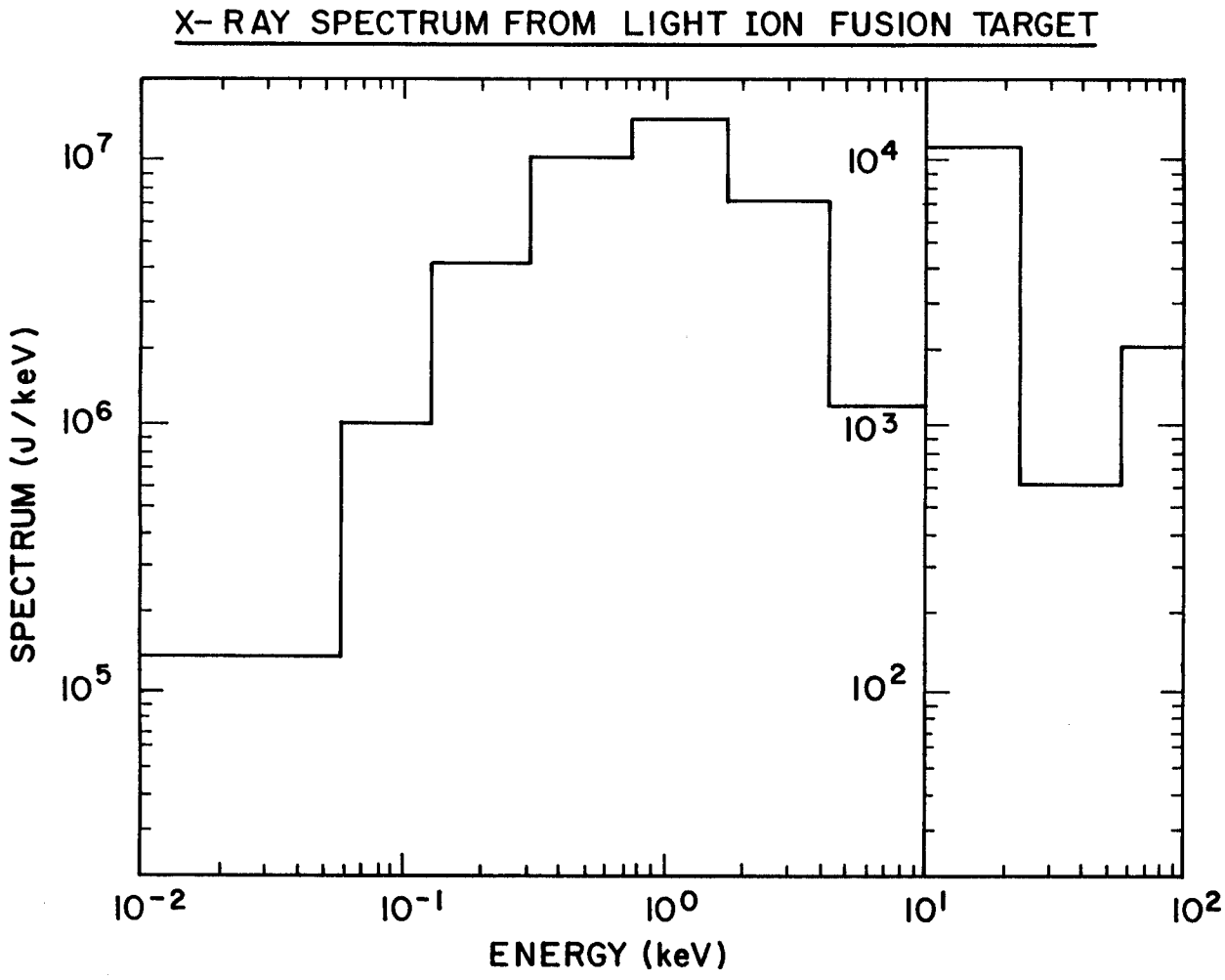

Fig. 5. LIB target x-ray spectrum.

distribution in the gas. The code also models the slowing down of the ions in the gas and uses this as an energy and momentum source term in the gas dynamics equations. For our target design we assumed that all of the ion energy was in the form of lead and neglected the other ionic species of the target. These calculations were done for two types of gases: argon and nitrogen. In both cases we assumed a pressure of 10 torr. This is believed to be the pressure required to support z-pinch plasma channel formation.

The faceplate of the diagnostics package was assumed to be 1 meter from the target. In Fig. 6 we show the x-ray spectrum at the faceplate in a chamber filled with 10 torr of argon gas. On this figure we also show the target x-ray spectrum at the surface of the target. (Note the change of vertical scale at E = 10 keV in this and the following figure.) Table 3 summarizes all of the various loadings on the faceplate. This 357 J/cm^2 of soft x-rays represents a very severe surface heat loading on any component positioned at 1 meter from the target. The maximum overpressure is 5.4 MPa. In the case of nitrogen gas shown in Fig. 7, the hard x-ray component is greater due to reduced attenuation in the lower-Z gas. The reradiated component is somewhat less, 274 J/cm^2, but the overpressure is much greater, 20 MPa. This large overpressure places severe constraints on the mechanical strength of the faceplate. In general, the nitrogen gas transmits a greater fraction of the hard (> 1 keV) prompt x-rays than the argon. The argon produces a significantly higher soft x-ray fluence than the nitrogen.

4. Gamma Ray and Neutron Interaction with the Diagnostics Package

Neutron and gamma ray transport calculations have been done for various faceplate materials to determine the spectrum behind the faceplate. These simple calculations were done using the ANISN code for the one-dimensional

Table 3. Fluences on the Detector at 1 Meter for Argon and Nitrogen

Gas Type	Energy Density Hard X-Rays	Energy Density Soft X-Rays	Energy Density γ-Rays	Energy Density Neutrons	Max ΔP
	(J/cm^2)	(J/cm^2)	(J/cm^2)	(J/cm^2)	MPa
Ar	9.8	357	2.4	1144	5.4
N_2	176	274	2.4	1144	20.

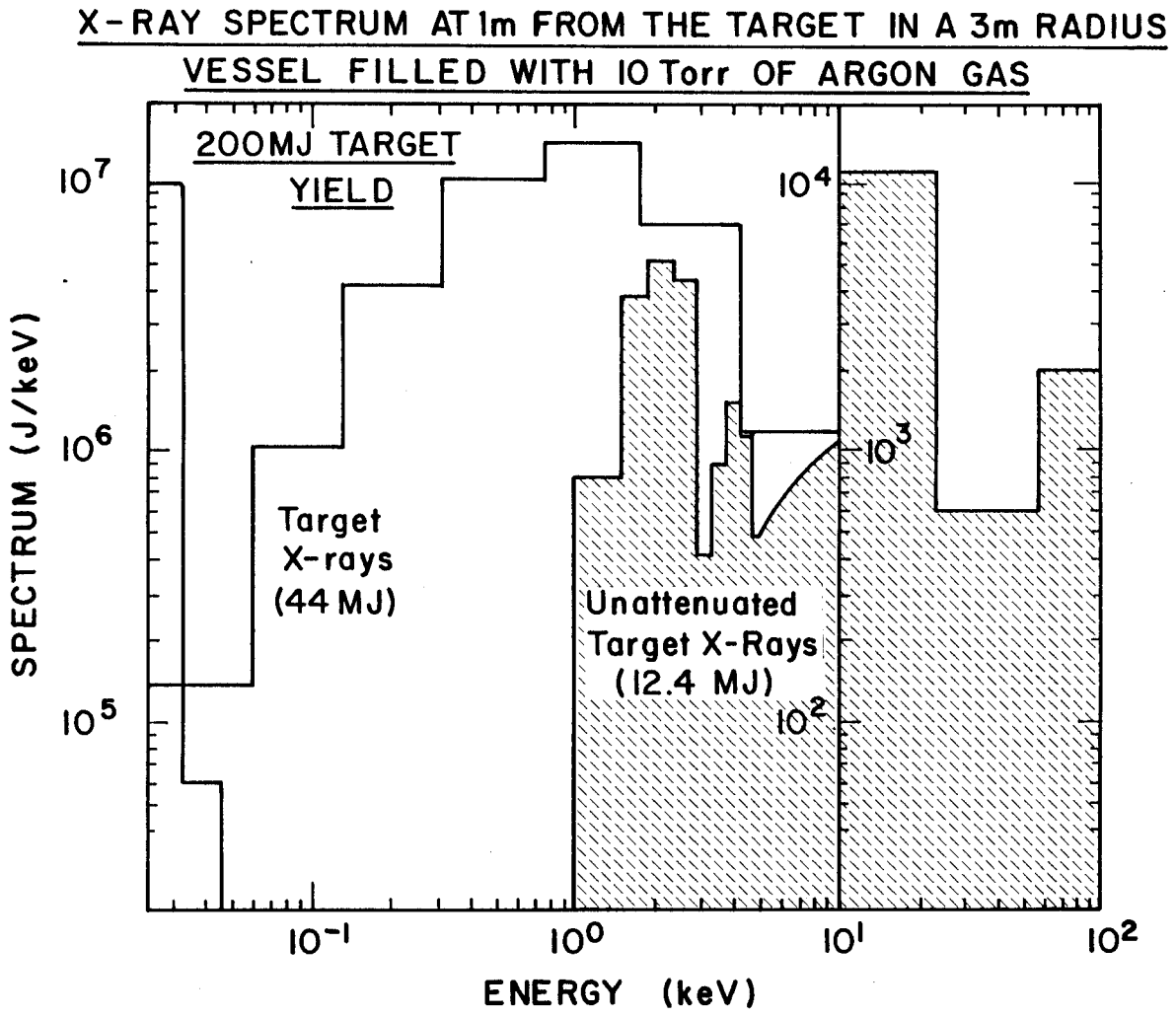

Fig. 6. X-ray spectrum at the diagnostics package faceplate with argon gas attenuation.

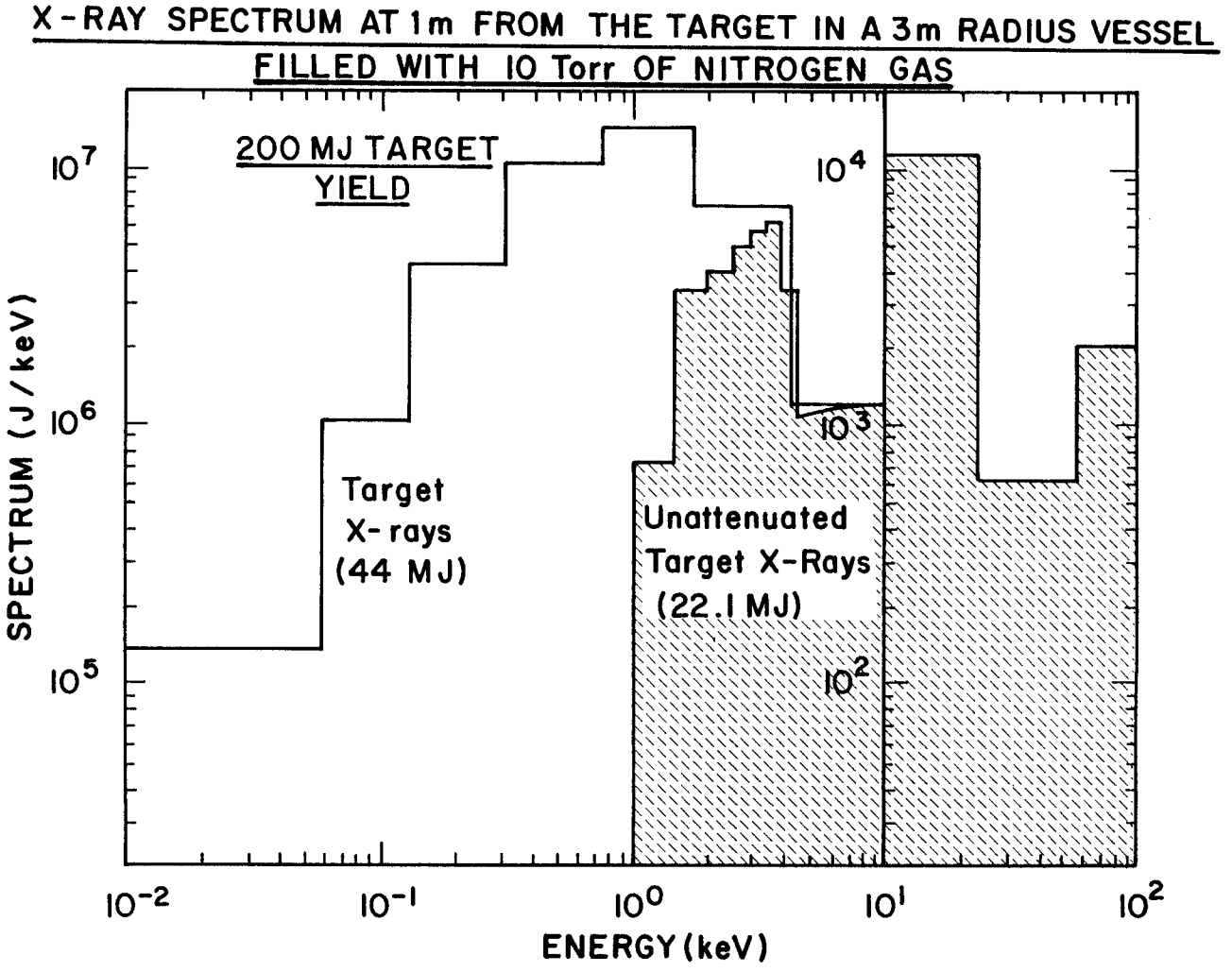

Fig. 7. X-ray spectrum at the diagnostics package faceplate with nitrogen gas attenuation.

geometry shown in Fig. 8 and the input spectra given in Figs. 3 and 4. The results are summarized in Table 4. They are normalized to 1 D-T fusion neutron per second. Since this is a steady state calculation, care must be taken in interpreting it for the highly transient target explosion. Relative spectral information is most important to this discussion and the steady state calculation will accurately supply this information.

In all cases, the neutron flux behind the faceplate is actually larger than the flux in front of it. This is due to the (n,2n) reactions in the faceplate dominating over the very slight $1/R^2$ effect between the front and the back. Table 4 indicates that the fraction of neutrons at 14.1 MeV (in the 1st group) falls dramatically from the front to the back of the faceplate. The spectrum of neutrons in these three cases is plotted in Figs. 9 to 13. Figure 9 compares the neutron spectrum behind a 1 cm aluminum faceplate, with and without the effect of reflection from the contents of the diagnostic package, the back faceplate, and the first wall and shield. With reflection included there is a much greater number of neutrons in the low energy continuum. Figure 10 shows the same behavior for a 5 cm thick aluminum faceplate. Figure 11 shows little difference between the 1 and 5 cm cases. Figures 12 and 13 compare the neutron spectra behind 1 and 5 cm aluminum and steel faceplates. In each case the steel produces more neutrons in the intermediate energy range but the aluminum shows a greater thermal component. The thermal component in the steel is suppressed due to greater absorption. In all of these cases, when compared with the uncollided flux at the front of the diagnostics package (Fig. 14), the spectrum behind the faceplate is softer, but with a pronounced 14.1 MeV peak. This peak can be easily discriminated and with corrections can serve as a reliable neutron diagnostic.

Table 4. Neutron and Gamma Flux in the TDF Diagnostics Package

	Neutron Flux	% at 14.1 MeV	Gamma Flux
Uncollided flux at front of faceplate	8.32×10^{-6}	70%	1.39×10^{-7}
Flux behind faceplate			
1 cm Al 6061 - no reflection	9.29×10^{-6}	47%	3.67×10^{-6}
1 cm Al 6061 - with reflection	3.84×10^{-5}	11.4%	1.81×10^{-5}
5 cm Al 6061 - no reflection	9.02×10^{-6}	33%	5.53×10^{-6}
5 cm Al 6061 - with reflection	3.74×10^{-5}	8%	1.69×10^{-5}
1 cm - 2-1/4 Cr-1 Mo	7.26×10^{-5}	5.8%	2.06×10^{-5}
5 cm - 2-1/4 Cr-1 Mo	6.92×10^{-5}	3.4%	1.52×10^{-5}

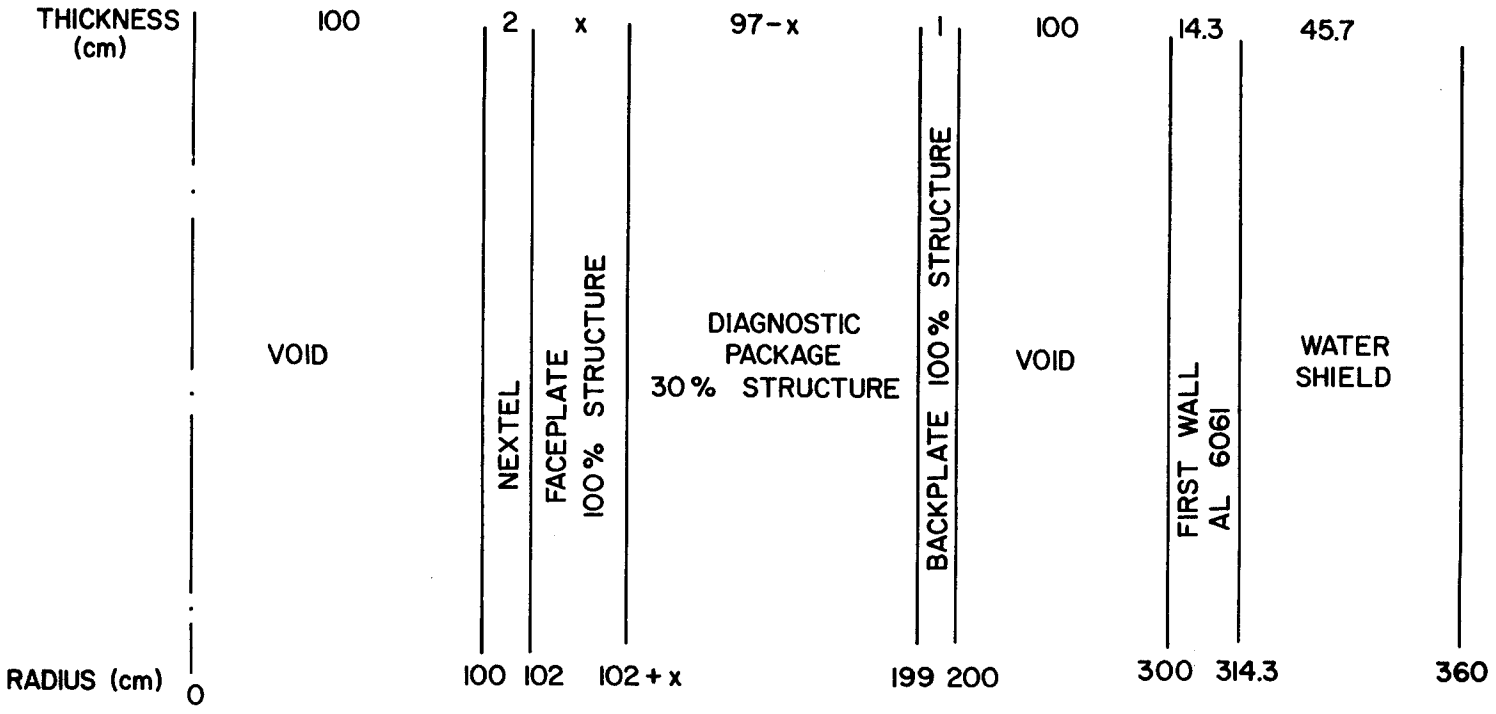

DIAGNOSTIC PACKAGE STRUCTURE : AL 6061 OR $2\frac{1}{4}$Cr IMo STEEL
FIREPLATE THICKNESS : 1 OR 5 cm

Fig. 8. One-dimensional geometry used for neutronics calculations.

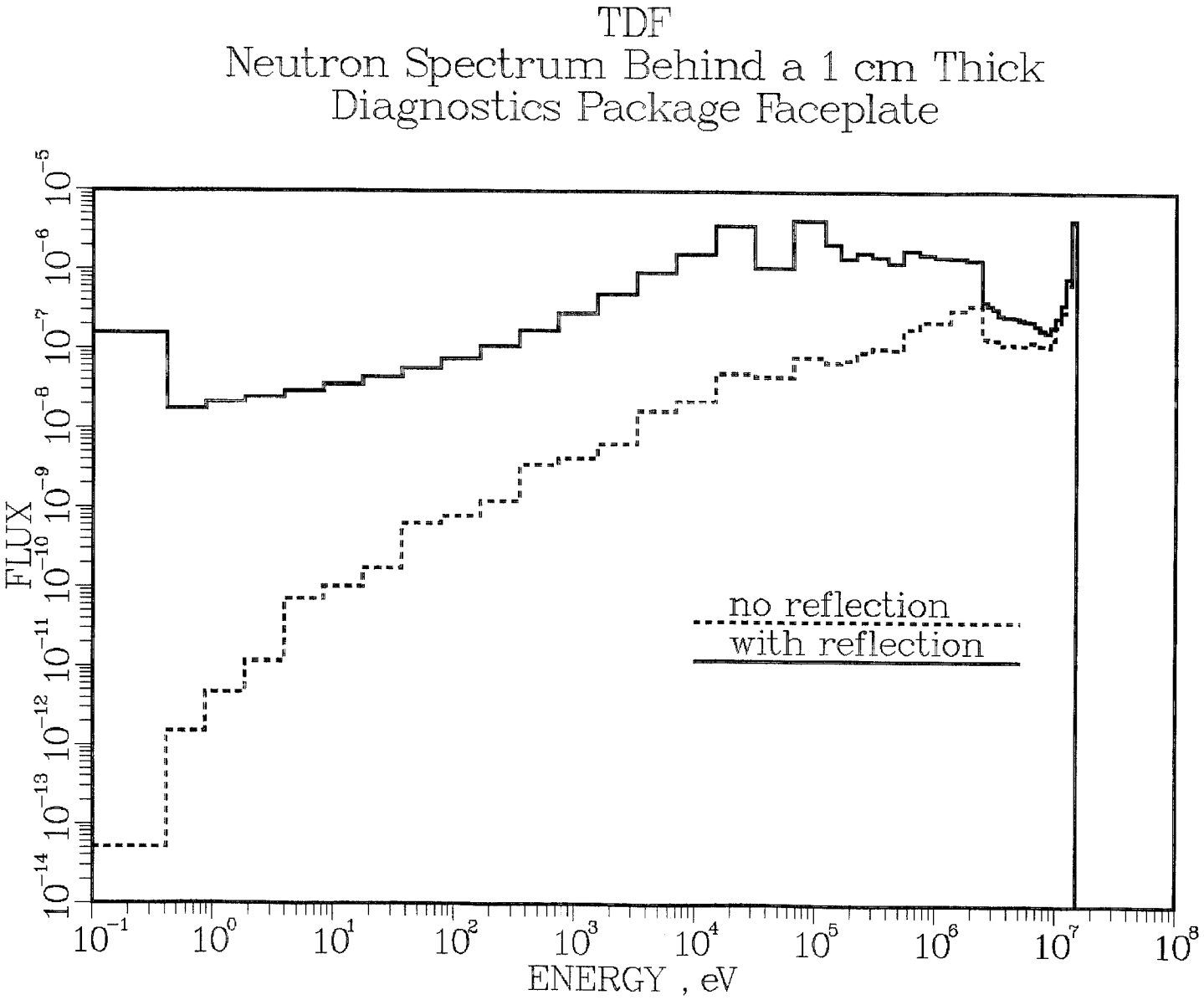

Fig. 9. Neutron flux behind 1 cm Al faceplate with and without reflected neutrons.

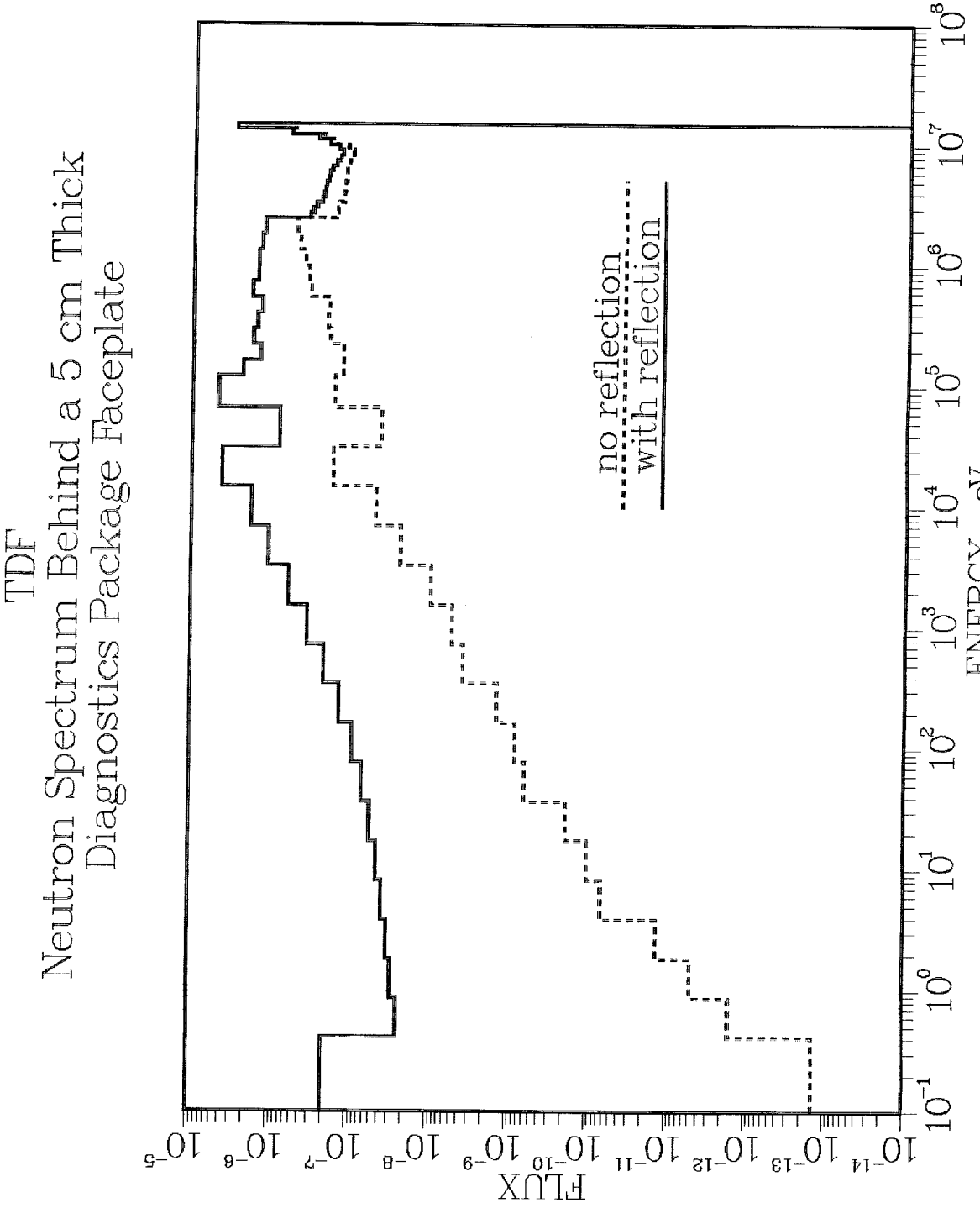

Fig. 10. Neutron flux behind 5 cm Al faceplate with and without reflected neutrons.

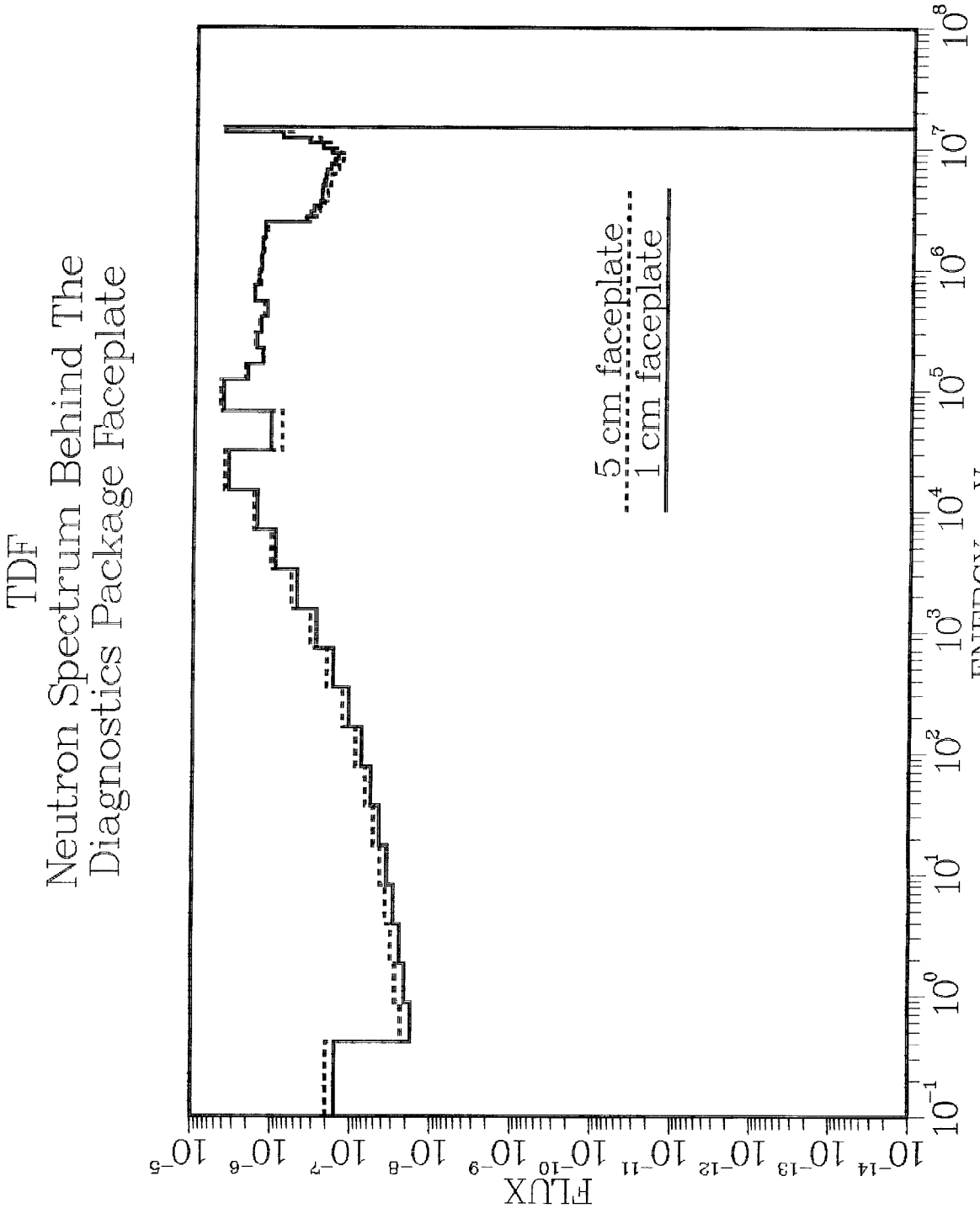

Fig. 11. Comparison of neutron spectra for 1 and 5 cm faceplates.

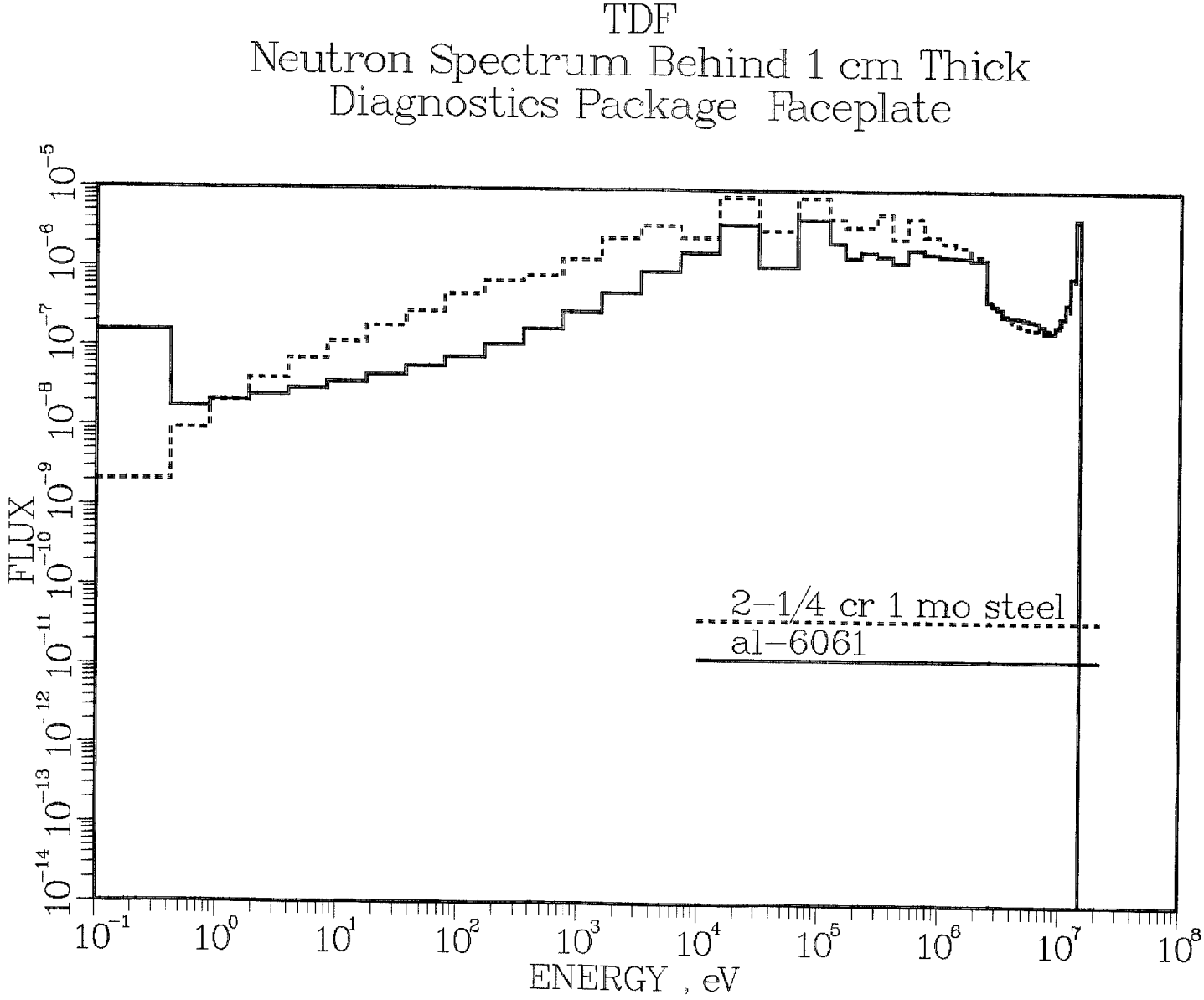

Fig. 12. Neutron fluxes behind 1 cm faceplates of Al 6061 and 2-1/4 Cr-1 Mo steel.

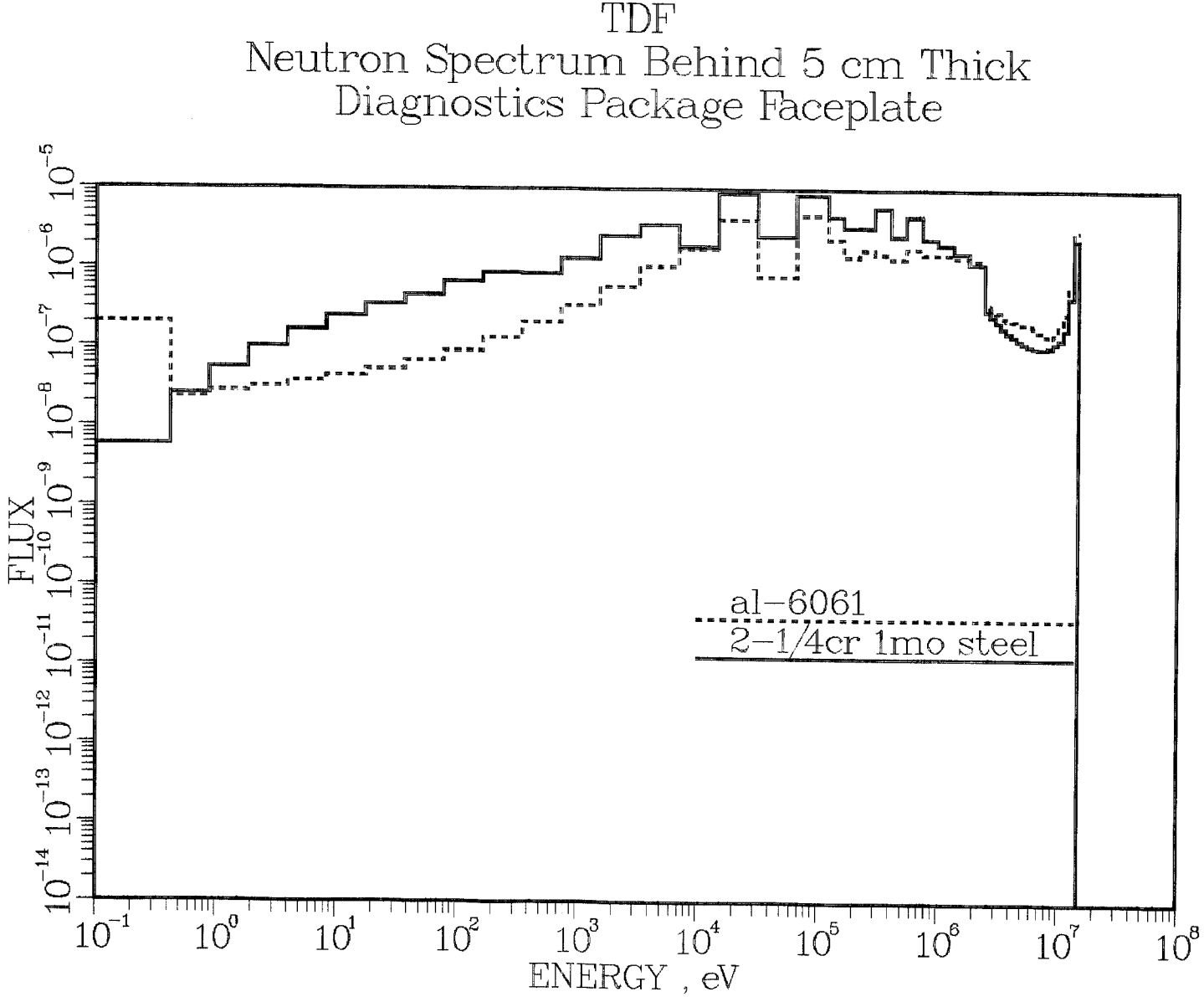

Fig. 13. Neutron fluxes behind 5 cm faceplates of Al 6061 and 2-1/4 Cr-1 Mo steel.

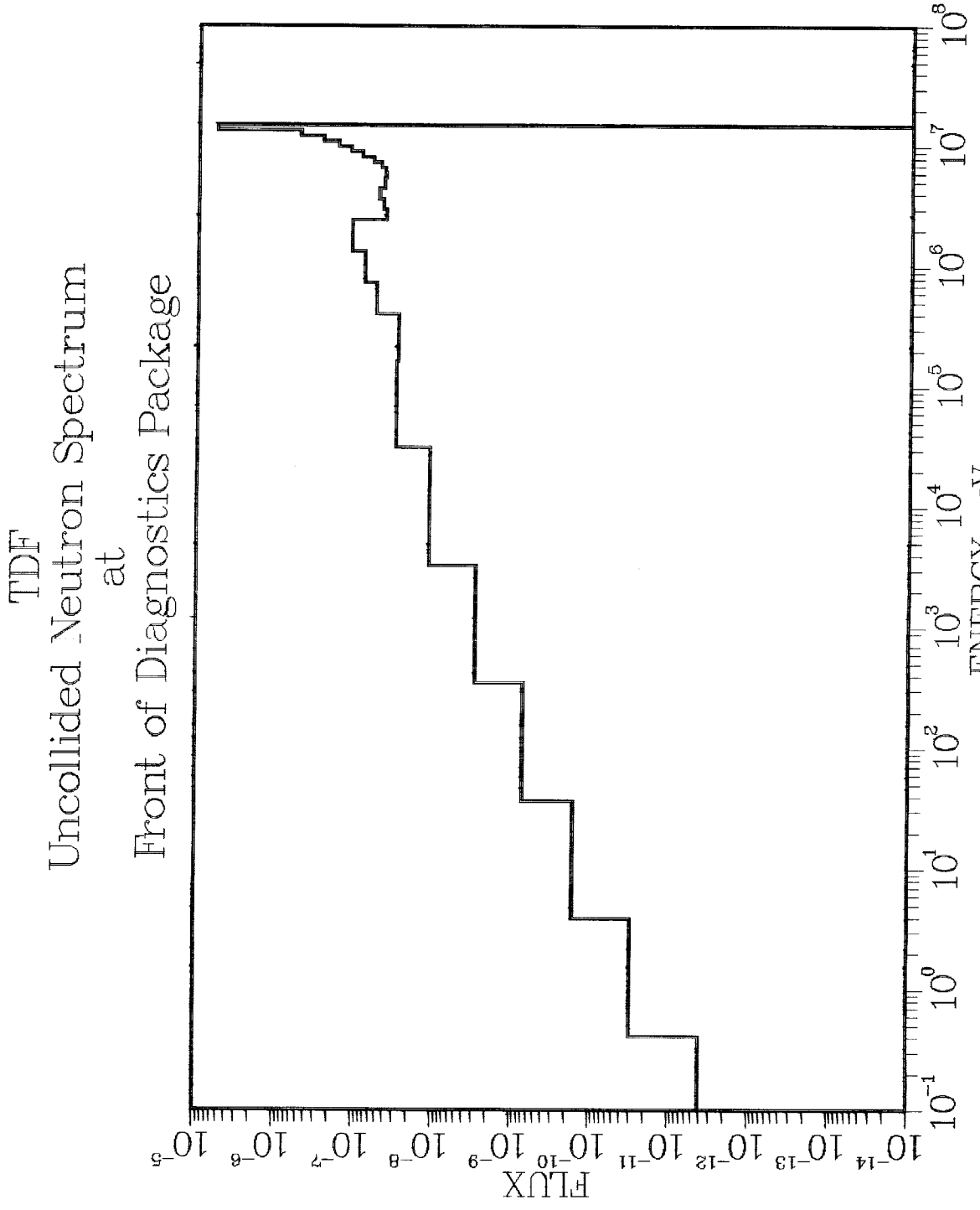

Fig. 14. Uncollided neutron flux at the front of the faceplate.

The significant amount of inelastic neutron collisions in the faceplate and the rest of the TDF, greatly affects the gamma ray spectrum in the diagnostics package. Table 4 indicates that for a 1 cm aluminum faceplate the gamma flux behind the faceplate is 2 orders of magnitude greater than the uncollided flux. Hence the signal to noise ratio for the gammas is very small unless the detector can somehow discriminate between direct target gammas and those derived from subsequent neutron interactions. Similar figures to those given for neutrons are given for the gamma spectrum in Figs. 15 to 20. A comparison of Fig. 15 with the others shows the greatly increased gamma flux over the uncollided value. It also shows the softening of the gamma flux. Figures 16 and 17 show the effect of including gammas due to interaction with the diagnostics and the remainder of the TDF. Figure 18 indicates that the difference between 1 and 5 cm of aluminum is not great on the gamma flux while Figs. 19 and 20 show that the differences between aluminum and steel are greater. However, the most significant effect is the increase in gamma flux by one to two orders of magnitude over the uncollided value. This indicates that the use of gamma ray diagnostics for target implosion and burn will be difficult unless the primary gammas can be discriminated. This might be possible using time discrimination. The "secondary" gammas are primarily due to neutron interactions that come 10 ns after the primary gamma burst. This indicates that such diagnostics might be better placed far from the target to enhance the time of flight neutron lag.

On the other hand, if gammas are to be used to test radiation hardening of electronics, then the two order of magnitude increase in gamma flux is beneficial. In this case, Table 4 shows that 1 cm of steel produces the greatest gamma flux of all those cases tried.

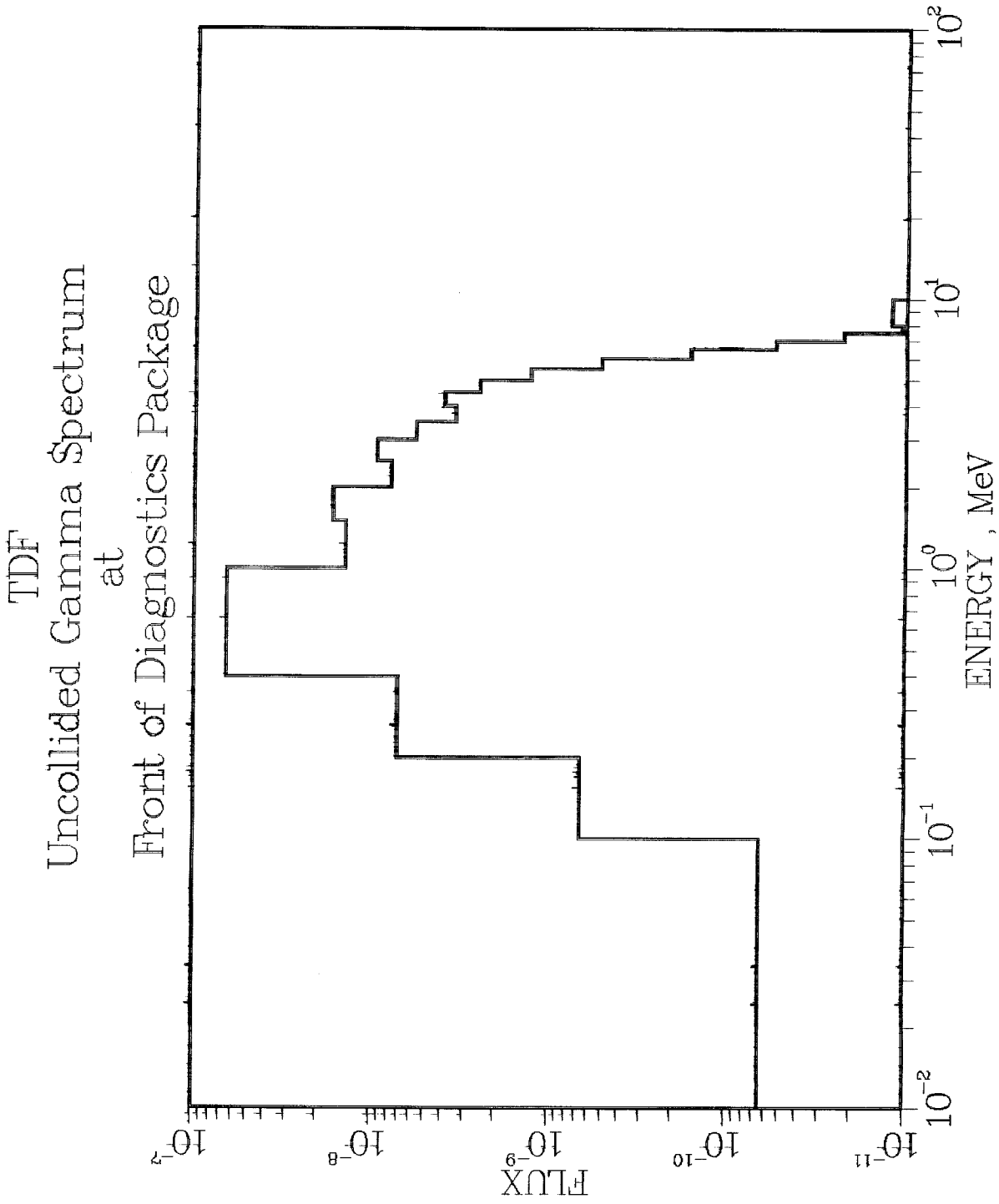

Fig. 15. Uncollided gamma flux at the front of the faceplate.

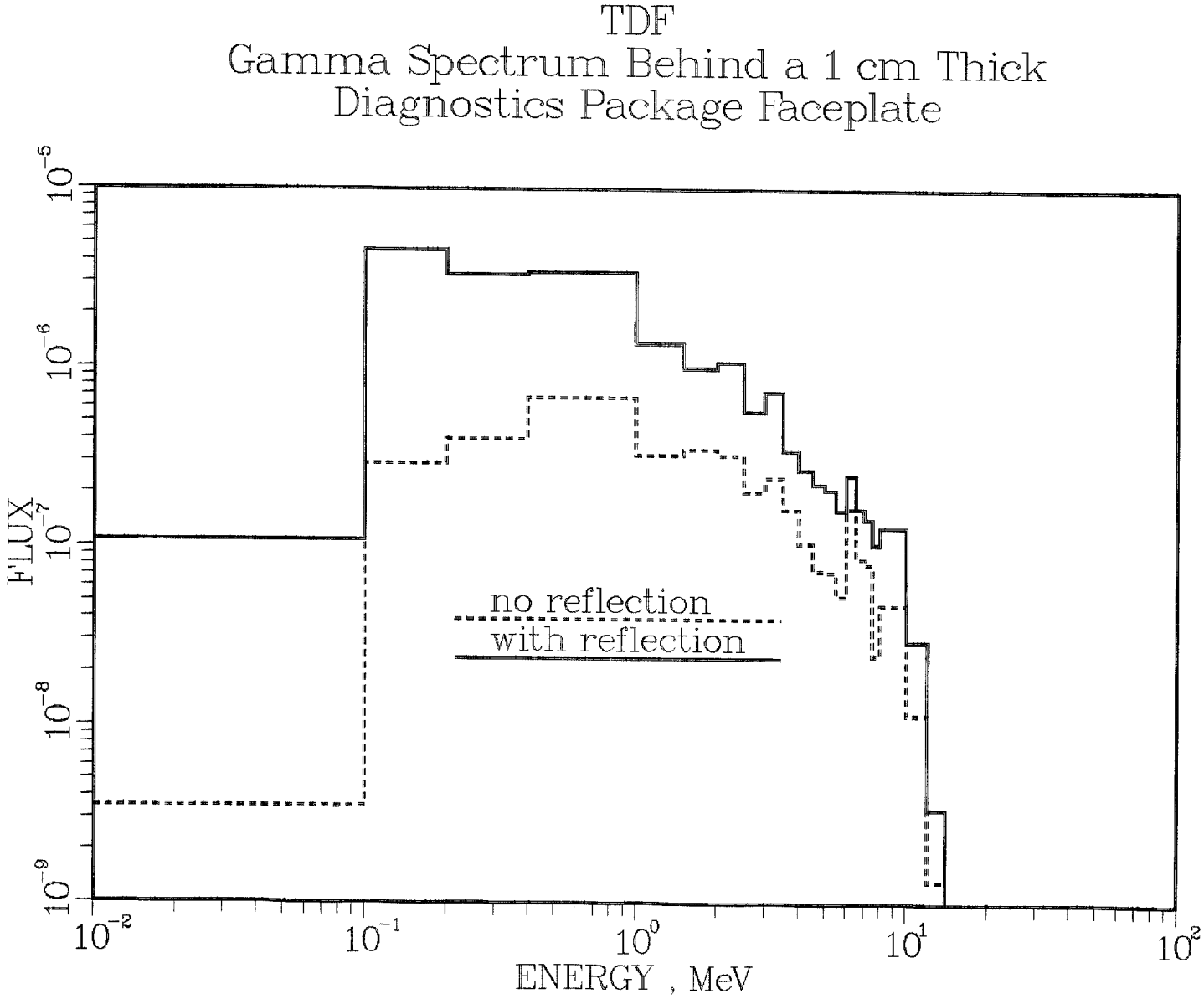

Fig. 16. Gamma flux behind 1 cm Al faceplate with and without neutron reflection.

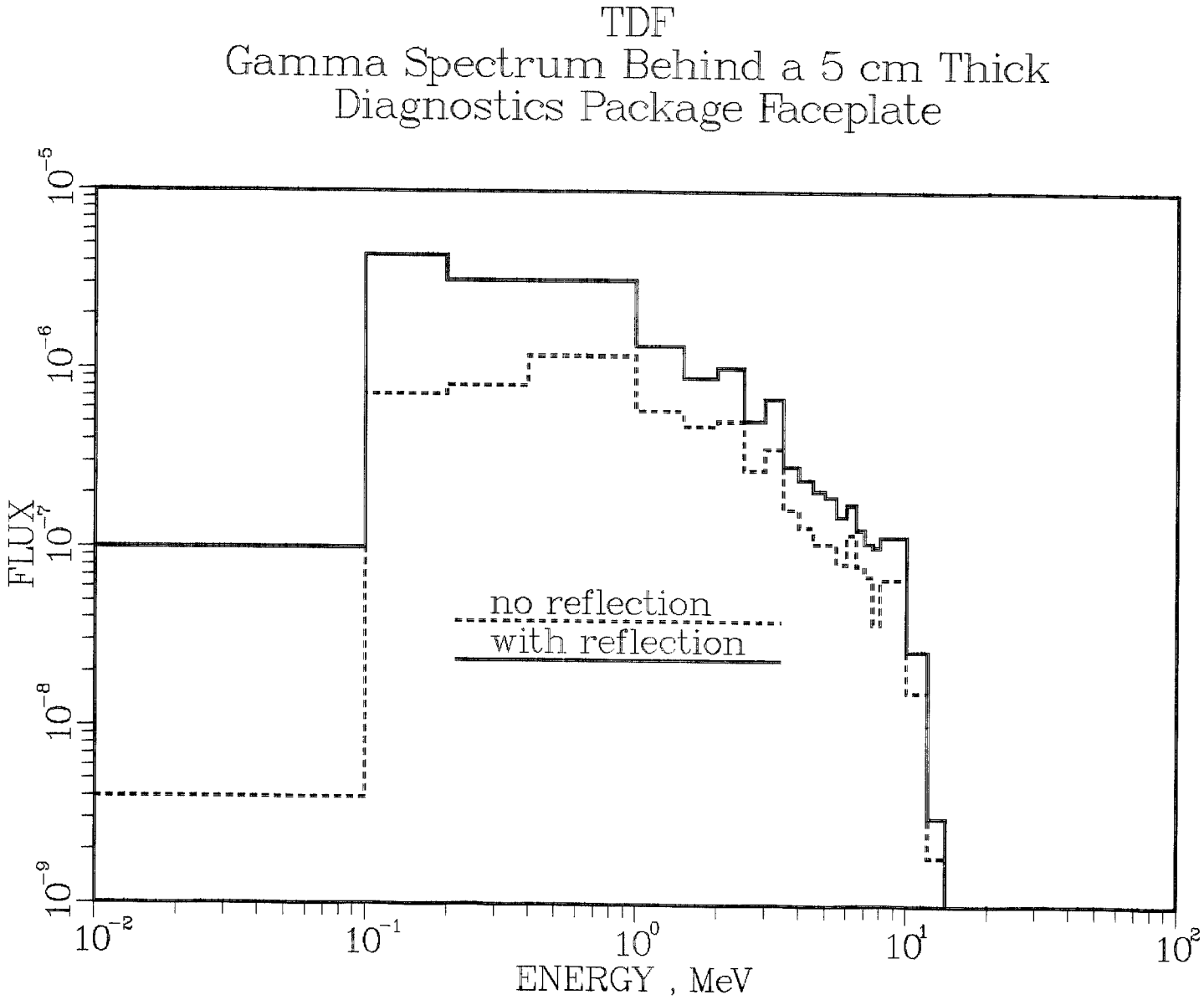

Fig. 17. Gamma flux behind 5 cm Al faceplate with and without neutron reflection.

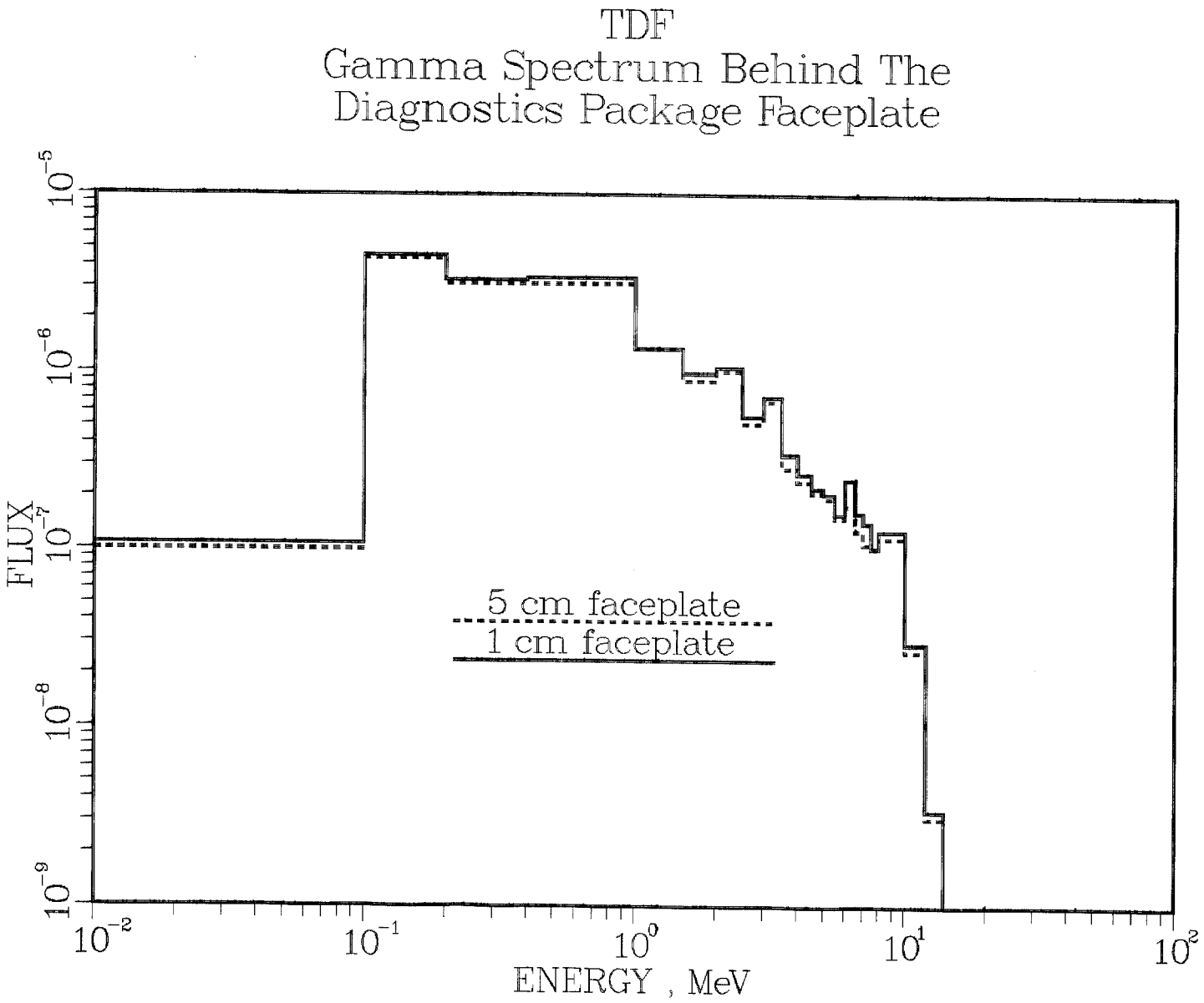

Fig. 18. Comparison of gamma fluxes behind 1 and 5 cm Al faceplates.

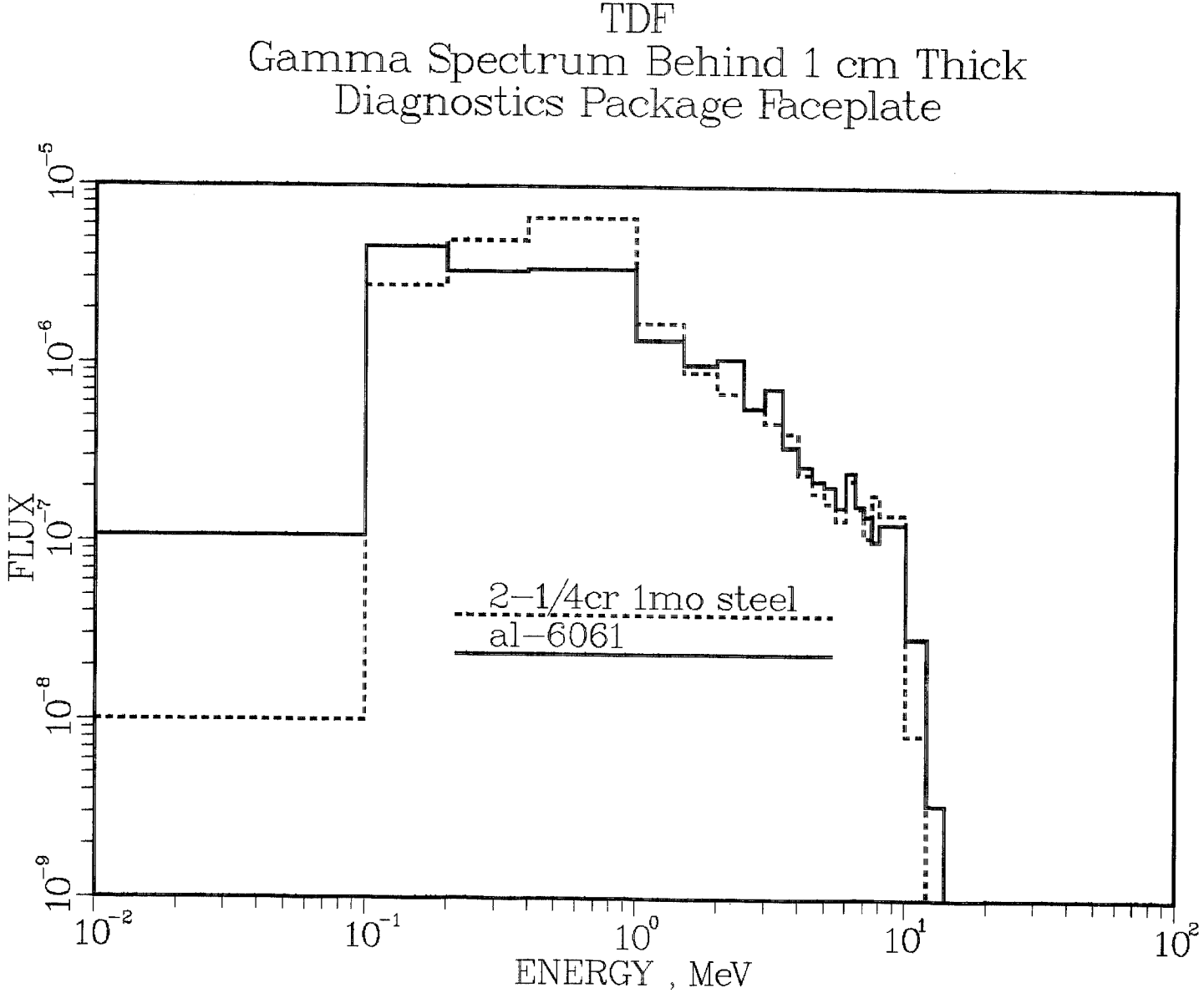

Fig. 19. Gamma fluxes behind 1 cm faceplates of Al 6061 and 2-1/4 Cr-1 Mo steel.

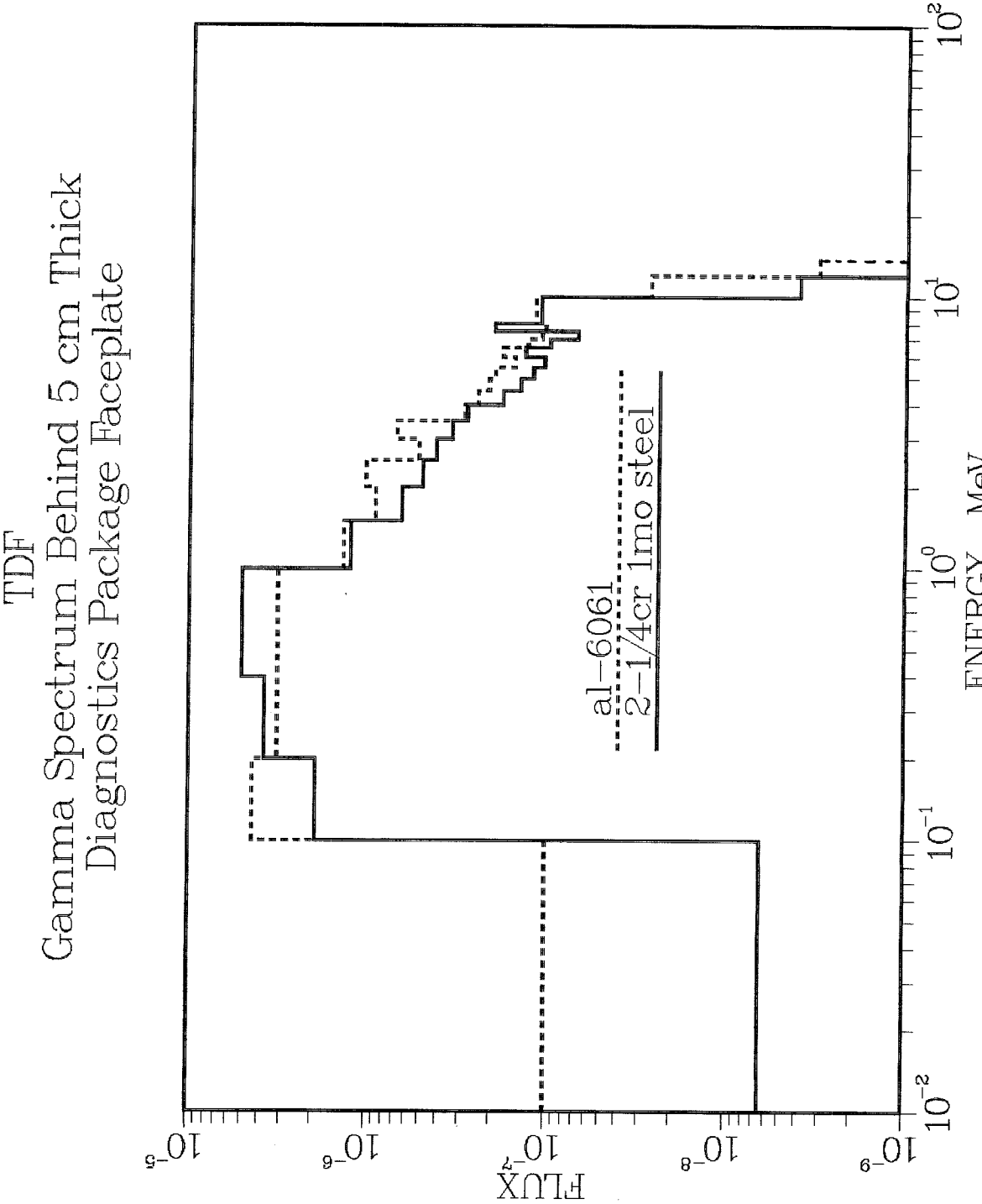

Fig. 20. Gamma fluxes behind 5 cm faceplates of Al 6061 and 2-1/4 Cr-1 Mo steel.

5. Protection of the Target Diagnostics from the Heat Flux and Overpressure

The vessel containing the diagnosing instruments must be designed to protect these instruments from the thermal and mechanical effects of the blast. The heat flux experienced by the diagnostics package is severe when the front of the package is positioned 1 meter from the target explosion. Whereas the NEXTEL[13] thermal liner on the first wall is designed to survive a 200 MJ target shot without melting, the thermal shield on the diagnostics package is allowed to partially melt on each shot. This is permitted because the diagnostics package will only be in the target chamber for 50 shots before it is removed and the thermal shield is replaced. The overpressure due to the target explosion is borne by an aluminum or steel plate in back of the thermal shield. Once again, the design constraints are reduced because the plate must only survive 50 shots and fatigue is ignored so that the maximum allowed stress is the yield stress. The required thicknesses of the thermal and mechanical shields have been determined on the basis of calculations of their response to the blast.

The intense heat flux on the thermal shield is mainly in the form of low energy photons from the fireball created by the target explosion. This can be modeled as a constant surface heat flux within a short pulse. The melting of the shield has been modeled with the THWACK finite difference conduction and change of phase computer code. The calculation is summarized in Table 5, where one sees that it represents the response of the shield to a 200 MJ explosion 1 meter away in the presence of an argon cavity gas. The argon case is presented here because it imposes the highest radiant energy density on the shield. An additional conservative feature of this calculation is that it is assumed that any material that melts instantly leaves the surface and absorbs

Table 5. Melting of NEXTEL Liner on Diagnostics Package

General Parameters	
Target Yield	200 MJ
Distance from Target to Diagnostics	1 m
Cavity Gas	Argon
Initial Boundary Conditions	
Initial Temperature	300 K
Radiant Energy Density	357 J/cm^2
Duration of Pulse	10^{-6} s
Heat Flux	3.57×10^5 kW/cm^2
Properties of NEXTEL	
Mass Density	2.7 g/cm^3
Thermal Conductivity	5.1×10^{-4} W/cm-K
Melting Point	2073 K
Phase Change Energy (melting)	756 J/g
Heat Capacity	1 J/g-K
Code Predictions	
Melt Thickness/Shot	3.5×10^{-2} cm
Melt Thickness/50 Shots	1.75 cm
Energy Going into Melting/Shot	71.5 J/cm^2
Sensible Heat/Shot	167.6 J/cm^2
Energy Conducted Away from Surface/Shot	117.9 J/cm^2

no additional energy. This calculation shows that a 2 cm thick NEXTEL shield will conservatively protect the diagnostics package from heat for 50 shots.

The mechanical response is dependent on the dimensions of the diagnostics package transverse to the propagation of the blast wave.

6. Faceplate Mechanical Stress

For this scoping study, it is tentatively assumed that the diagnostics unit has a solid circular faceplate. It is also assumed that the edge is securely attached to the supporting structure and thus maximum mechanical stress will be radial, at the outer edge. Since fatigue is not an issue in this application, the design criterion was simple yielding of the material. Two metals were considered, Al 6061-T6 and 2-1/4 Cr-1 Mo. It should be noted that other alloys with higher strength, as well as nonmetallic composites could be used. In addition, a stronger faceplate could be designed using double wall construction, ribbing, etc.

In Fig. 21 results are presented such that one can identify the faceplate thickness and diameter to withstand a given dynamic pressure. The curves for the two materials are similar since the yield strengths for the steel and aluminum alloys are very close at room temperature, i.e. 256 and 272 MPa, respectively. The vertical scale on the left is generic but the right scale corresponds to the dynamic pressure for the previously described case of 200 MJ in nitrogen. For this, the results indicate that an aluminum faceplate located 1.0 meter from the target could sustain the predicted overpressure of 20 MPa with thicknesses of 1 cm and 5 cm if the diameters did not exceed 6 cm and 30 cm, respectively.

It appears that the design of the diagnostics unit faceplate can be developed without any unusual difficulties.

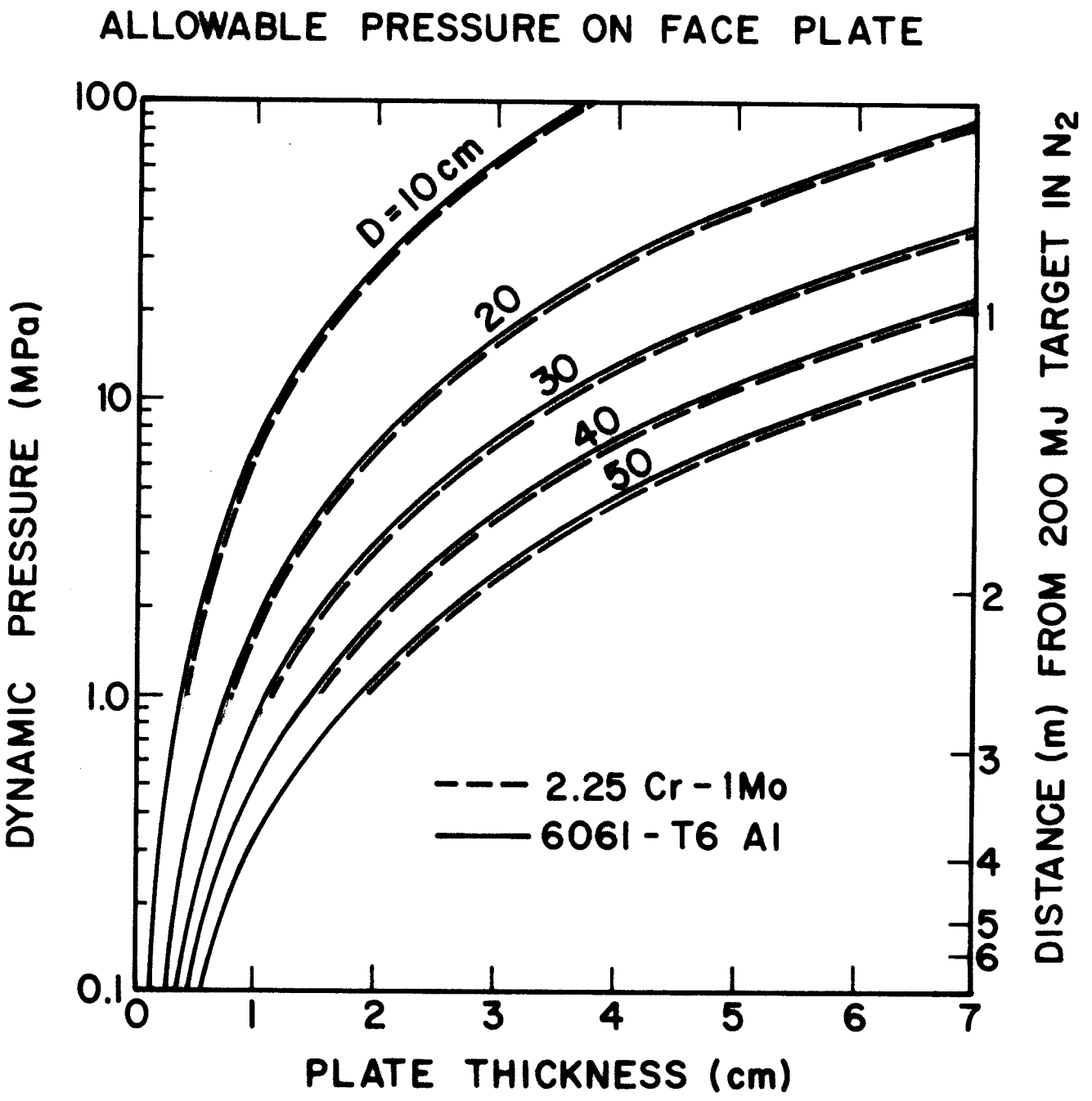

Fig. 21 Allowable pressure on diagnostics package faceplate.

7. Possible Diagnostics for High Yield LIF Targets

New diagnostic methods will be required to determine the implosion and burn dynamics of high yield LIF targets. The following are a few ideas in this regard.

An important problem during target implosion is the timing of the input power with the collapse time of the target. Should there be multiple shells one would also like to know the collision time of the shells. This might be accomplished using 14 MeV neutron signals as the diagnostic. If the buffer gas between the shells is DT, calculations done at LANL using LASNEX show that temperatures in this gas during collision of the shells is sufficient to produce countable numbers of neutrons. Precise time measurement of this signal could serve as an indication of the collision time. The timing of this signal and the number of neutrons produced could be easily compared with hydrodynamic simulations and could indicate the presence of shell breakup or mixing during collision.

The density attained by different target layers during implosion is an important design quantity. This could be determined by neutron activation of seed materials in each layer and subsequent activation analysis of captured debris. In this case the diagnostics package would be designed to capture a precise fraction of debris for quantitative analysis.

A cleaner method of measuring density might be to use the gamma rays from specific inelastic neutron scattering events as the measure of interaction rate and thus density. Small quantities of different seed materials in each layer of interest would probably provide good signals, considering the strength of the neutron source.

Acknowledgement

Support for this work has been provided by the U.S. Department of Energy.

References

1. G. Moses, R. Peterson, R. Engelstad, E. Lovell, G. Kulcinski, K. O'Brien, A. White, J. Watrous, D. Cook, "Light Ion Fusion Target Development Facility Preconceptual Design," Nucl. Tech./Fusion 4, 961 (1983).

2. J.R. Freeman, L. Baker and D.L. Cook, "Plasma Channels for Intense Light Ion Beam Reactors," Nucl. Fusion 22, 383 (1982).

3. G.A. Moses and R.R. Peterson, "First Wall Protection in Particle Beam Fusion Reactors," Nucl. Fusion 20, 849 (1980).

4. R.R. Peterson, G.W. Cooper and G.A. Moses, "Cavity Gas Analysis for Light Ion Beam Fusion Reactors," Nucl. Tech./Fusion 1, 377 (1981).

5. R.R. Peterson, K.J. Lee and G.A. Moses, "Low Density Cavity Gas Fireball Dynamics in the Light Ion Beam Fusion Target Development Facility," Proc. of 9th Symp. on Engr. Prob. of Fusion Res., Chicago, IL, Oct. 1981, p. 668.

6. R. Bangerter, "Laser Program Annual Report - 1976," Lawrence Livermore National Laboratory Report UCRL-50021-76, pp. 4-44.

7. B. Badger et al., "HIBALL - A Conceptual Heavy Ion Beam Driven Fusion Reactor Study," University of Wisconsin Fusion Technology Institute Report UWFDM-450, June 1981, p. III.1-1.

8. G.A. Moses, G.R. Magelssen, R. Israel and T. Spindler, "PHD-IV, A Plasma Hydrodynamics, Thermonuclear Burn, Radiative Transfer Computer Code," University of Wisconsin Fusion Technology Institute Report UWFDM-194 (revised January 1982).

9. RSIC Code Package CCC-254, "ANISN-ORNL," Radiation Shielding Information Center, Oak Ridge National Laboratory, Oak Ridge, TN.

10. M.E. Sawan, G.A. Moses and G.L. Kulcinski, "Time Dependent Neutronics Analysis for the HIBALL Heavy Ion Beam Fusion Reactor," Nucl. Tech./Fusion 2, 215 (1982).

11. G.A. Moses, T.J. McCarville and R.R. Peterson, "Documentation for MF-FIRE, A Multifrequency Radiative Transfer Version of FIRE," University of Wisconsin Fusion Technology Institute Report UWFDM-458, March 1982, to be published in Computer Physics Communications.

12. R.R. Peterson and G.A. Moses, "MIXERG, An Equation of State and Opacity Computer Code," Comp. Phys. Comm. 28, 405 (1983). Also, University of Wisconsin Fusion Technology Institute Report UWFDM-464, March 1982.

13. NEXTEL is a tradename of 3M Corporation for 62% Al_2O_3, 24% SiO_2 and 14% B_2O_3 ceramic fibers that are available in a number of different fabrics.